

Including the Fermion Vacuum Fluctuations in the $(2 + 1)$ flavor Polyakov Quark Meson Model

Sandeep Chatterjee ^{*} and Kirtimaan A. Mohan [†]

Centre for High Energy Physics, Indian Institute of Science, Bangalore, 560012, India.

Abstract

We consider the $(2 + 1)$ flavor Polyakov Quark Meson Model and study the effect of including fermion vacuum fluctuations on the thermodynamics and phase diagram. The resulting model predictions are compared to the recent QCD lattice simulations by the HotQCD and Wuppertal-Budapest collaborations. The variation of the thermodynamic quantities across the phase transition region becomes smoother. This results in better agreement with the lattice data. Depending on the value of the mass of the sigma meson, including the vacuum term results in either pushing the critical end point into higher values of the chemical potential or excluding the possibility of a critical end point altogether.

PACS numbers: 12.38Aw, 12.39.-x, 12.38.Gc, 05.70.-a

1 Introduction

With the advent of ultrarelativistic heavy ion experiments such as RHIC (BNL), LHC (CERN) and the planned future CBM experiment at the FAIR facility in Darmstadt, research on the properties of strongly interacting matter has entered into a fascinating era. Quantum Chromodynamics (QCD) which is the theory of strong interactions predicts that at high temperature and baryon density normal hadronic matter undergoes phase transition to a chirally symmetric phase of Quark Gluon Plasma (QGP) [1–5].

QCD at this temperature and density is a strongly coupled theory and hence one cannot use perturbative methods to study the details of this phase transition. Non-perturbative methods like first principle Lattice QCD (LQCD) Monte Carlo simulations give us important insights into various aspects of the phase transition. However LQCD suffers from the notorious sign problem at non zero baryon density [6, 7]. Although several methods have been developed [6, 7] to bypass the sign problem at small baryon chemical potential μ_B , a satisfactory solution to the sign problem for all values of μ_B still eludes us. An alternate approach is to study various phenomenological models whose phase diagrams possess the essential features of QCD. These models serve to complement LQCD calculations and may provide us with an intuitive understanding about regions of the phase diagram currently inaccessible to LQCD.

The QCD Lagrangian for N_f flavors of massless quarks has the global symmetry $SU_L(N_f) \times SU_R(N_f)$ which spontaneously breaks into $SU_V(N_f)$ in the low energy hadronic vacuum by the formation of chiral condensate together with $N_f^2 - 1$ massless Goldstone bosons. In the opposite limit of infinite quark mass, QCD becomes a pure $SU(3)$ gauge theory. The low energy vacuum that possesses a center symmetry $Z(3)$ under the color gauge group (confined phase) gets spontaneously broken in the high temperature/baryon density regime (deconfined phase). The Polyakov loop which is vanishing in the confining phase and becomes non zero in the symmetry broken phase serves as the order parameter of the confinement-deconfinement phase transition [8]. In real life we have dynamical quarks with non zero masses and hence neither of the symmetries discussed above are exact. Thus the chiral condensate and the Polyakov loop only serve as approximate order parameters for the chiral phase transition and confinement-deconfinement phase transition respectively.

^{*}sandeep@cts.iisc.ernet.in

[†]kirtimaan@cts.iisc.ernet.in

There have been numerous attempts to study the QCD phase diagram using effective chiral models like the Nambu-Jona-Lasinio (NJL) [9–12], linear sigma [13–15] and the quark-meson (QM) [16] models. These models possess QCD like chiral symmetry breaking pattern. Later, variants of these were developed to incorporate the confinement-deconfinement transition, namely PNJL [17–20], PLSM and PQM [21, 22] models. There is a basic difference in the mechanism of chiral symmetry breaking in the QM/PQM models compared to NJL/PNJL models. In the latter case, the fermion vacuum term which is the contribution due to the infinite Dirac fermion sea causes the symmetry breaking. In QM/PQM models, the spontaneous symmetry breaking is generated by the mesonic potential and the fermion vacuum term is usually neglected. Recently in the 2 flavor PQM model it has been shown that the order of the phase transition in the massless limit changes from first order to crossover on adding the vacuum term [23] which also modifies the shape of the isentropic trajectories near the critical end point (CEP) [24]. In yet another study in the presence of a magnetic field [25], the phase diagram is shown to be considerably affected by the vacuum term. More recently, the effect of the vacuum term in the 2 flavor case on the thermodynamics as well as the phase diagram was extensively studied [26].

In this paper we will consider the PQM model together with the vacuum term (PQMVT) in the $(2+1)$ flavor case. We first compute the thermodynamic potential in the presence of the vacuum term. Then we calculate thermodynamic quantities like energy density ϵ , pressure p , entropy s , conformal symmetry breaking measure Δ , speed of sound c_s^2 and specific heat capacity c_V . We also compute several second order quark number susceptibilities (QNS). In each case we compare our results with those obtained from LQCD and comment on the modification in the model prediction due to the addition of the vacuum term. We also present the phase diagram of PQMVT in the $T - \mu_B$ plane. The organisation of the paper is as follows: In Sec. 2, we discuss the details of the PQMVT model and its parameters. In Sec. 3 we present our results and elucidate the effect of the vacuum term on thermodynamics and phase diagram of PQMVT. Finally, we summarise and conclude in Sec. 4.

2 The Model

We will be working in the generalized three flavor quark meson linear sigma model which has been combined with the Polyakov loop potential [22, 27, 28]. In this model, quarks denoted by $q_f = (u, d, s)^T$ come in $N_f = 3$ flavor and $N_c = 3$ color degrees of freedom and are coupled to the $SU_L(3) \times SU_R(3)$ symmetric mesonic fields M as well as a spatially constant temporal gauge field A^μ . Our starting point is the following model Lagrangian

$$\mathcal{L} = \text{Tr}(\partial_\mu M^\dagger \partial^\mu M) + \bar{q}_f(i\gamma^\mu D_\mu - gM_5)q_f - \mathcal{U}_M(M) - \mathcal{U}_P(\Phi, \bar{\Phi}, T), \quad (1)$$

where nine mesons in the scalar ($\sigma_a, J^P = 0^+$) and pseudoscalar ($\pi_a, J^P = 0^-$) sectors are together put into the 3×3 complex matrices M and M_5 given by

$$M = T_a \xi_a = T_a(\sigma_a + i\pi_a) \quad (2)$$

$$M_5 = T_a \xi_{5a} = T_a(\sigma_a + i\gamma_5 \pi_a) \quad (3)$$

where $T_a = \frac{\lambda_a}{2}$ represent the 9 generators of $U(3)$ with $\lambda_0 = \sqrt{\frac{2}{3}} \mathbf{1}$. The generators follow $U(3)$ algebra $[T_a, T_b] = if_{abc}T_c$ and $\{T_a, T_b\} = d_{abc}T_c$ where f_{abc} and d_{abc} are standard antisymmetric and symmetric structure constants respectively with $f_{ab0} = 0$ and $d_{ab0} = \sqrt{\frac{2}{3}} \mathbf{1} \delta_{ab}$ and are normalized as $\text{Tr}(T_a T_b) = \frac{\delta_{ab}}{2}$.

In (1), $\mathcal{U}_M(M)$ and $\mathcal{U}_P(\Phi, \bar{\Phi}, T)$ are the mesonic and Polyakov loop potentials respectively. Polyakov loop field $\Phi(\vec{x})$ is defined as the thermal expectation value of color trace of the Wilson loop in the temporal direction

$$\Phi(\vec{x}) = \frac{1}{N_c} \langle \text{Tr}_c L(\vec{x}) \rangle, \quad (4)$$

where $L(\vec{x})$ is a matrix of the $SU_c(3)$ color gauge group.

$$L(\vec{x}) = \mathcal{P} \exp \left[i \int_0^\beta d\tau A_0(\vec{x}, \tau) \right] \quad (5)$$

Here \mathcal{P} denotes path ordering, A_0 is the temporal vector field and $\beta = T^{-1}$ [8]. Also, $\bar{\Phi} = \frac{1}{N_c} \langle \text{Tr}_c L^\dagger(\vec{x}) \rangle$ is the Hermitean conjugate of Φ . The coupling of quarks with the gauge field is implemented through the covariant derivative

$D_\mu = \partial_\mu - iA_\mu$ and $A_\mu = \delta_{\mu 0}A_0$ (Polyakov gauge), where $A_\mu = g_s A_\mu^a \lambda^a / 2$. λ_a are the Gell-Mann matrices in the color space where the index a runs from $1 \cdots 8$ and g_s is the $SU_c(3)$ gauge coupling. g is the flavor blind Yukawa coupling that couples the three quark flavors with the mesons σ_a and π_a of the meson matrix M_5 .

The mesonic potential $\mathcal{U}_M(M)$ has the following form

$$\begin{aligned} \mathcal{U}_M(M) = & m^2 \text{Tr}(M^\dagger M) + \lambda_1 [\text{Tr}(M^\dagger M)]^2 \\ & + \lambda_2 \text{Tr}(M^\dagger M)^2 - c [\det(M) + \det(M^\dagger)] \\ & - \text{Tr}[H(M + M^\dagger)]. \end{aligned} \quad (6)$$

While the 't Hooft determinant term breaks explicitly the $U(1)_A$ symmetry, the $SU_L(3) \times SU_R(3)$ chiral symmetry is explicitly broken by $H = T_a h_a$ and the ξ field picks up a non zero vacuum expectation value $\bar{\xi}$. In order to give the correct vacuum quantum numbers after chiral symmetry breakdown, h_0 , h_3 and h_8 are the only allowed non zero parameters in H . In this work we retain isospin symmetry which further sets $h_3 = 0$. This leads to the 2 + 1 flavor symmetry breaking scenario with nonzero condensates $\bar{\sigma}_0$ and $\bar{\sigma}_8$.

The effective Polyakov loop potential $\mathcal{U}_P(\Phi, \bar{\Phi}, T)$ is constructed to reproduce the thermodynamics of pure gauge theory on the lattice. The simplest $Z(3)$ symmetric polynomial form based on a Ginzburg-Landau ansatz is given by [19]

$$\frac{\mathcal{U}_{\text{Poly}}(\Phi, \bar{\Phi}, T)}{T^4} = -\frac{b_2(T)}{2} \Phi \bar{\Phi} - \frac{b_3}{6} (\Phi^3 + \bar{\Phi}^3) + \frac{b_4}{4} (\Phi \bar{\Phi})^2. \quad (7)$$

Later an improved ansatz was proposed [29, 30] by including the VanderMonde term which is the Jacobian of transformation from the matrix valued field L to the complex valued field Φ . Here we closely follow [30]

$$\frac{\mathcal{U}_{\text{Poly-VM}}(\Phi, \bar{\Phi}, T)}{T^4} = \frac{\mathcal{U}_{\text{Poly}}(\Phi, \bar{\Phi}, T)}{T^4} - \kappa \log [1 - 6\Phi \bar{\Phi} + 4(\Phi^3 + \bar{\Phi}^3) - 3(\Phi \bar{\Phi})^2]. \quad (8)$$

The logarithm term constrains the Φ and $\bar{\Phi}$ values to smaller than 1. Details of the above mentioned model parameters will be discussed in Section 2.2.

2.1 Grand Potential

The grand canonical partition function for a spatially uniform system in thermal equilibrium at finite temperature T and quark chemical potential $\mu_f (f = u, d, s)$ is given by

$$\begin{aligned} \mathcal{Z} &= \text{Tr} \exp[-\beta(\hat{\mathcal{H}} - \sum_{f=u,d,s} \mu_f \hat{\mathcal{N}}_f)] \\ &= \int \prod_a \mathcal{D}\sigma_a \mathcal{D}\pi_a \int \mathcal{D}q \mathcal{D}\bar{q} \exp \left[-\int_0^\beta d\tau \int_V d^3x \left(\mathcal{L}^\mathcal{E} + \sum_{f=u,d,s} \mu_f \bar{q}_f \gamma^0 q_f \right) \right]. \end{aligned} \quad (9)$$

where V is the three dimensional volume of the system, and $\beta = \frac{1}{T}$. In general, the quark chemical potentials corresponding to the three conserved flavors up(u), down(d) and strange(s) are different. In the 2 + 1 flavor setup, the $SU_V(2)$ symmetry is unbroken and thus the quark chemical potentials for u and d quarks become equal $\mu_u = \mu_d = \mu_x$ while the strange quark chemical potential is $\mu_s = \mu_y$.

We evaluate \mathcal{Z} in the mean-field approximation [31, 32]. In this approximation, thermal and quantum fluctuations of the meson fields are neglected and are replaced by their expectation values $\langle M \rangle = T_0 \langle \sigma_0 \rangle + T_8 \langle \sigma_8 \rangle$ while quarks and antiquarks are retained as quantum fields. Now following the standard procedure [18, 19, 21, 33] one can obtain the expression of the grand potential as a sum of a pure gauge field contribution $\mathcal{U}_P(\Phi, \bar{\Phi}, T)$, a meson contribution $\mathcal{U}_M(\langle M \rangle)$ and a quark-antiquark contribution $\Omega_{\bar{q}q}$

$$\Omega(T, \mu_x, \mu_y) = -\frac{T \ln \mathcal{Z}}{V} = \mathcal{U}_M(\langle M \rangle) + \mathcal{U}_P(\Phi, \bar{\Phi}, T) + \Omega_{\bar{q}q} \quad (10)$$

In order to study the 2 + 1 flavor case, a more convenient basis is the nonstrange-strange (x, y) basis obtained from the original singlet-octet (0,8) basis by the following basis transformation,

$$\begin{pmatrix} v_x \\ v_y \end{pmatrix} = \frac{1}{\sqrt{3}} \begin{pmatrix} \sqrt{2} & 1 \\ 1 & -\sqrt{2} \end{pmatrix} \begin{pmatrix} v_0 \\ v_8 \end{pmatrix} \quad (11)$$

applied on the scalar, pseudoscalar mesons and external fields, that is $v \in \{\sigma, \pi, h\}$. In this new basis the nonstrange and strange quarks and antiquarks decouple and the quark masses become

$$m_x = g \frac{\sigma_x}{2}, \quad m_y = g \frac{\sigma_y}{\sqrt{2}} \quad (12)$$

The mesonic potential in this nonstrange-strange basis reads,

$$\begin{aligned} U(\sigma_x, \sigma_y) &= \mathcal{U}_M(\langle M \rangle) \\ &= \frac{m^2}{2} (\sigma_x^2 + \sigma_y^2) - h_x \sigma_x - h_y \sigma_y - \frac{c}{2\sqrt{2}} \sigma_x^2 \sigma_y \\ &\quad + \frac{\lambda_1}{2} \sigma_x^2 \sigma_y^2 + \frac{1}{8} (2\lambda_1 + \lambda_2) \sigma_x^4 \\ &\quad + \frac{1}{8} (2\lambda_1 + 2\lambda_2) \sigma_y^4, \end{aligned} \quad (13)$$

while the quark-antiquark contribution is given by,

$$\Omega_{\bar{q}q} = \Omega_{\bar{q}q}^v + \Omega_{\bar{q}q}^{\text{th}} \quad (14)$$

where

$$\Omega_{\bar{q}q}^v = -2N_c \sum_{f=u,d,s} \int \frac{d^3p}{(2\pi)^3} E_f \quad (15)$$

$$\Omega_{\bar{q}q}^{\text{th}} = -2T \sum_{f=u,d,s} \int \frac{d^3p}{(2\pi)^3} [\ln g_f^+ + \ln g_f^-] \quad (16)$$

g_f^+ and g_f^- are defined after taking trace over color space

$$\begin{aligned} g_f^+ &= \left[1 + 3\Phi e^{-E_f^+/T} + 3\bar{\Phi} e^{-2E_f^+/T} + e^{-3E_f^+/T} \right] \\ g_f^- &= \left[1 + 3\bar{\Phi} e^{-E_f^-/T} + 3\Phi e^{-2E_f^-/T} + e^{-3E_f^-/T} \right] \end{aligned} \quad (17)$$

Here we use the notation $E_f^\pm = E_f \mp \mu_f$ where E_f is the single particle energy of a quark/antiquark.

$$E_f = \sqrt{p^2 + m_f^2} \quad (18)$$

At zero temperature and chemical potentials, $\Omega_{\bar{q}q}$ gets a contribution only from $\Omega_{\bar{q}q}^v$. This is the fermion vacuum contribution which is usually neglected. We shall study the effect of this term on the thermodynamics. Employing dimensional regularisation to regularise the diverging integral in (15), we obtain [23, 26]

$$\Omega_{\bar{q}q}^v = \Omega_{\bar{q}q}^{\text{reg}}(\Lambda) = -\frac{N_c}{8\pi^2} \sum_{f=u,d,s} m_f^4 \log \left[\frac{m_f}{\Lambda} \right] \quad (19)$$

where Λ is the regularisation scale parameter. In Appendix A, we show that the thermodynamic potential is independent of Λ . Thus all physical observables are independent of the choice of Λ [23].

The quark condensates $\langle \sigma_x \rangle$, $\langle \sigma_y \rangle$ and the Polyakov loop expectation values $\langle \Phi \rangle$, $\langle \bar{\Phi} \rangle$ are obtained by searching for a global minima of the grand potential at a given value of temperature T and chemical potentials μ_x and μ_y ,

$$\left. \frac{\partial \Omega}{\partial \sigma_x} = \frac{\partial \Omega}{\partial \sigma_y} = \frac{\partial \Omega}{\partial \Phi} = \frac{\partial \Omega}{\partial \bar{\Phi}} \right|_{\sigma_x=\langle \sigma_x \rangle, \sigma_y=\langle \sigma_y \rangle, \Phi=\langle \Phi \rangle, \bar{\Phi}=\langle \bar{\Phi} \rangle} = 0. \quad (20)$$

2.2 Model Parameters

The model parameters are fixed by inputs from lattice and experiments. The parameters of the mesonic potential namely m^2 , λ_1 , λ_2 , c , g , h_x and h_y are fixed by using the following experimentally known quantities as in [15, 32]: pion mass m_π and pion decay constant f_π , kaon mass m_K and kaon decay constant f_K , average squared mass of η and η' mesons, $(m_\eta^2 + m_{\eta'}^2)$ and sigma mass m_σ . g is fixed by using a light quark constituent mass $m_x = 300$ MeV in (12). This gives a strange quark constituent mass $m_s \approx 433$ MeV. It turns out that λ_2 is the only parameter that depends on Λ . However, this dependence cancels with that of $\Omega_{qq}^{\text{reg}}(\Lambda)$ to yield a Λ independent thermodynamic potential. Thus, Λ is an arbitrary parameter here and we do not need any further experimental input to fix it. In Appendix A we discuss in detail the fixing of these parameters. Experimentally the mass of the σ meson m_σ lies in the range 400 – 1200 MeV [34] while recent studies point to $m_\sigma \sim 400 - 500$ MeV [35]. All our results are obtained with $m_\sigma = 400$ MeV. In Table 1, we have given the parameters used in this work.

We now discuss the parameters of the gauge potentials $\mathcal{U}_{\text{Poly}}(\Phi, \bar{\Phi}, T)$ and $\mathcal{U}_{\text{Poly-VM}}(\Phi, \bar{\Phi}, T)$ used in this work.

$$\frac{\mathcal{U}_{\text{Poly-VM}}(\Phi, \bar{\Phi}, T)}{T^4} = \frac{\mathcal{U}_{\text{Poly}}(\Phi, \bar{\Phi}, T)}{T^4} - \kappa \log \left[1 - 6\Phi\bar{\Phi} + 4(\Phi^3 + \bar{\Phi}^3) - 3(\Phi\bar{\Phi})^2 \right] \quad (21)$$

where $\mathcal{U}_{\text{Poly}}$ is given by

$$\frac{\mathcal{U}_{\text{Poly}}(\Phi, \bar{\Phi}, T)}{T^4} = -\frac{b_2(T)}{2}\Phi\bar{\Phi} - \frac{b_3}{6}(\Phi^3 + \bar{\Phi}^3) + \frac{b_4}{4}(\Phi\bar{\Phi})^2. \quad (22)$$

Here $b_2(T)$ is given by

$$b_2(T) = a_0 + a_1 \frac{T_0}{T} + a_2 \left(\frac{T_0}{T} \right)^2 + a_3 \left(\frac{T_0}{T} \right)^3 \quad (23)$$

The parameters of $b_2(T)$, b_3 and b_4 are obtained by fitting to the pure gauge lattice data in [19].

$$\begin{aligned} a_0 &= 6.75, & a_1 &= -1.95, & b_3 &= 0.75 \\ a_2 &= 2.625, & a_3 &= -7.44, & b_4 &= 7.5 \end{aligned}$$

The remaining parameters T_0 and κ are fixed by comparing the model predictions to lattice data of the full $(2+1)$ QCD. $T_0 = 270$ MeV is the phase transition temperature in the pure gauge theory. In the presence of dynamical quarks, fermionic contributions modify the running coupling of QCD [36, 37] which can be accounted for by a smaller value of T_0 [21, 36, 37]. While both HotQCD as well as WB groups agree that the chiral symmetry restoration takes place through a smooth crossover [38–41], there is still a disagreement on the relative values of T_χ and T_d , the transition temperatures associated with chiral and confinement-deconfinement crossovers respectively. The HotQCD lattice data [42, 43] with which we compare our model predictions show a coincidence of both transitions. On the other hand, WB sees $T_\chi < T_d$ [40, 44–46]. However, recently HotQCD have reported lower value of T_χ [47] which is in agreement with that of WB. We observe that by varying T_0 it is possible to change the relative values of T_χ and T_d in the model. We work with two values of T_0 : firstly, $T_0 = 270$ MeV. In this case $T_\chi < T_d$. We call this ModelWB. Secondly, $T_0 = 210$ MeV. In this case $T_\chi \simeq T_d$. We call this ModelHotQCD. The remaining parameter κ is adjusted to describe the lattice data of the scaled conformal symmetry breaking measure $\Delta/T^4 = (\epsilon - 3p)/T^4$. The two lattice groups differ in the height of the peak of Δ [44]: the peak height is about 50 % larger in HotQCD. Here we use different values of κ in ModelWB and ModelHotQCD to describe the WB and HotQCD data respectively. One could have obtained T_0 and κ by precision fitting of the LQCD data. Here we do not undertake such a procedure as the exact quantitative status is going to change as more refined LQCD data become available. Here we merely focus on comparing the trends between model and LQCD rather than exact matching. We summarise below the values of all the model parameters in Table 1.

| Model | m_σ [MeV] | m^2 [MeV ²] | λ_1 | $\lambda_2(\Lambda)$ | c | h_x [MeV ³] | h_y [MeV ³] | g | T_0 [MeV] | κ |
|-------------|------------------|---------------------------|-------------|----------------------|---------|---------------------------|---------------------------|-----|-------------|----------|
| ModelHotQCD | 400 | 80647.587 | -8.165 | 138.45 | 4801.95 | 1.785×10^6 | 3.805×10^7 | 6.5 | 210 | 0.1 |
| ModelWB | 400 | 80647.587 | -8.165 | 138.45 | 4801.95 | 1.785×10^6 | 3.805×10^7 | 6.5 | 270 | 0.2 |

Table 1: The parameter sets obtained with $\Lambda = 200$ MeV.

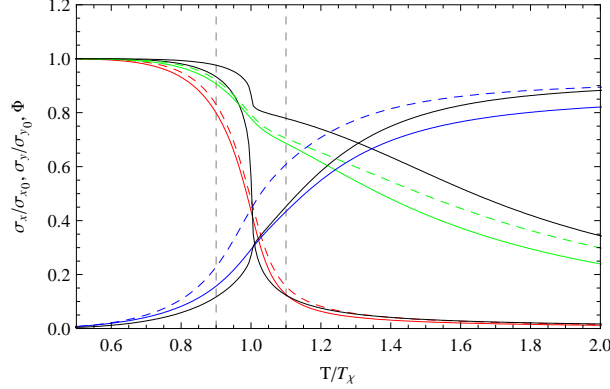


Figure 1: Plots of normalised $\langle\sigma_x\rangle$ (red), $\langle\sigma_y\rangle$ (green) and $\langle\Phi\rangle$ (blue) vs T/T_χ at $\mu_x = \mu_y = 0$ as obtained in PQMVT with $\mathcal{U}_{\text{Poly-VM}}$ as the Polyakov potential. The dashed curves refer to ModelHotQCD while the solid curves refer to ModelWB. The solid black curve in each case is obtained in PQM with the ModelWB parameter set.

3 Results

Having obtained the grand canonical potential $\Omega(T, \mu_x, \mu_y)$ in the presence of the vacuum term, we shall now compute various thermodynamic quantities and study the effect of inclusion of the vacuum term on these quantities. For a given (T, μ_x, μ_y) , at the mean field level, $\Omega(T, \mu_x, \mu_y)$ is only a function of the condensates σ_x , σ_y , Φ and $\bar{\Phi}$ which are determined by solving the gap equations (20) simultaneously. In Fig. (1) we have plotted the condensates $\langle\sigma_x\rangle$, $\langle\sigma_y\rangle$ and $\langle\Phi\rangle$ obtained in ModelHotQCD and ModelWB at zero chemical potentials ($\mu_x = \mu_y = 0$) with $\mathcal{U}_{\text{Poly-VM}}$ as the Polyakov potential. We do not plot $\langle\bar{\Phi}\rangle$ since at zero chemical potential $\langle\bar{\Phi}\rangle = \langle\Phi\rangle$. While the quark condensates come out similar in both the models, using a higher value of T_0 and κ in ModelWB results in a delayed confinement-deconfinement crossover as well as a suppressed value for the Polyakov condensate as compared to ModelHotQCD. For large T , $\langle\Phi\rangle$ in ModelWB falls short by 8% compared to that of ModelHotQCD. In order to compare the results between PQM and PQMVT, we have also plotted the results as obtained in PQM with the ModelWB parameter set. In PQM, $\langle\sigma_x\rangle$ drops sharply across the transition region accompanied by an unsmooth structure in $\langle\sigma_y\rangle$ and $\langle\Phi\rangle$. With the inclusion of the vacuum term, the drop in $\langle\sigma_x\rangle$ across the crossover is much more gentle and the jagged structures in the transition region in $\langle\sigma_y\rangle$ and $\langle\Phi\rangle$ are washed away. One can compare these condensates as obtained in PQMVT with those computed in LQCD.

In the left panel of Fig. 2, we have plotted the Polyakov condensate $\langle\Phi\rangle$ obtained for both the parameter sets with $\mathcal{U}_{\text{Poly-VM}}$ as the Polyakov potential and compared with LQCD [43, 45]. We have also plotted $\langle\Phi\rangle$ with $\mathcal{U}_{\text{Poly}}$ as the Polyakov potential and ModelWB as the parameter set for comparison. Although the VanderMonde term in $\mathcal{U}_{\text{Poly-VM}}$ suppresses the $\langle\Phi\rangle$ value, the model prediction is still much higher as compared to lattice. The use of a potential that yields first order phase transition in case of pure glue theory results in a more rapid rise of the Polyakov condensate not seen in lattice as also reported in PQM studies [28].

A direct comparison of $\langle\sigma_x\rangle$ and $\langle\sigma_y\rangle$ with lattice data is not possible. Unknown normalisation factors need to be first removed. One such observable with the desired chiral limit and which also acts as an order parameter for chiral symmetry breaking is [42, 43]

$$\Delta_{l,s}(T) = \frac{\langle\bar{\psi}\psi\rangle_{l,T} - \frac{\hat{m}_l}{\hat{m}_s} \langle\bar{\psi}\psi\rangle_{s,T}}{\langle\bar{\psi}\psi\rangle_{l,0} - \frac{\hat{m}_l}{\hat{m}_s} \langle\bar{\psi}\psi\rangle_{s,0}} \quad (24)$$

In our model computation, $\Delta_{l,s}$ will become [28]

$$\Delta_{l,s}(T) = \frac{\langle\sigma_x\rangle(T) - \left(\frac{h_x}{h_y}\right) \langle\sigma_y\rangle(T)}{\langle\sigma_x\rangle(0) - \left(\frac{h_x}{h_y}\right) \langle\sigma_y\rangle(0)} \quad (25)$$

In the right panel of Fig. 2, we present the comparison of $\Delta_{l,s}$ obtained in PQMVT with LQCD [43, 45, 46] for both the parameter sets. We also compare with results from PQM. A similar analysis made in [28] concluded that

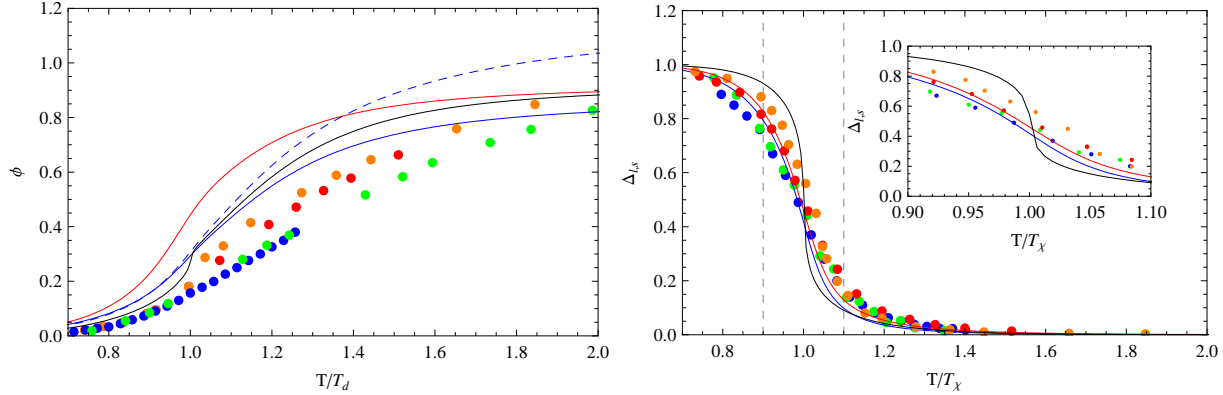


Figure 2: *Left*: Polyakov condensate $\langle \Phi \rangle$ obtained for ModelWB (solid blue) and ModelHotQCD (solid red) with the Polyakov potential $\mathcal{U}_{\text{Poly-VM}}$. The dashed blue curve is $\langle \Phi \rangle$ obtained in ModelWB with $\mathcal{U}_{\text{Poly}}$ as the Polyakov potential. For comparison we have also plotted $\langle \Phi \rangle$ obtained in PQM (solid black) with ModelHotQCD parameter set and $\mathcal{U}_{\text{Poly}}$ Polyakov potential. LQCD data from WB collaboration in blue (continuum estimate) and green ($N_\tau = 8$) [45] and from HotQCD group in red ($N_\tau = 8$ with asqtad action) and orange ($N_\tau = 8$ with p4 action) [43] are also shown. *Right*: Plots of $\Delta_{l,s}$ in ModelWB (blue) and ModelHotQCD (red) as obtained in PQMVT are shown. The black curve is the model prediction in PQM with ModelHotQCD parameter set. All the model predictions are obtained with the Polyakov potential $\mathcal{U}_{\text{Poly-VM}}$. For comparison LQCD data are also shown: WB continuum estimate in blue [45] and $N_\tau = 10$ [46] data in green are shown, the HotQCD data for $N_\tau = 8$ with p4 (orange) and asqtad (red) actions [43] are also shown.

the transition of $\Delta_{l,s}$ is sharper in PQM than that obtained in lattice. Here we find that the inclusion of the vacuum term in PQMVT makes the drop in $\Delta_{l,s}$ across the crossover region much more gentle. This leads to better agreement with lattice data. Thus the crossover transition becomes smoother with the addition of the vacuum term. We will see that the smooth variation of the condensates across the transition temperature also result in smooth variation of all thermodynamic quantities and has important consequence on the phase diagram as well.

3.1 $p, \epsilon, \Delta, s, c_v, c_s^2$

While on the lattice, the usual convention is to compute the trace of the energy momentum tensor [43] and extract the rest of the thermodynamic quantities from it, in model calculations a different approach is followed. Here it is natural to first compute the grand potential Ω with the values of the condensates obtained by solving (20). From Ω all the thermodynamic quantities can be easily obtained. The pressure of the system is given by

$$p(T, \mu_x, \mu_y) = -\Omega(T, \mu_x, \mu_y) \quad (26)$$

with the vacuum normalization $p(0, 0, 0) = 0$. The energy density ϵ is given by

$$\epsilon = -T^2 \frac{\partial(\Omega/T)}{\partial T} = -T \left(\frac{\partial \Omega}{\partial T} \right) + \Omega \quad (27)$$

while the entropy density s is now easily obtained from the thermodynamic relation at zero chemical potential

$$\epsilon = -p + Ts \quad (28)$$

Using (26) and (27), we can find the conformal symmetry breaking measure Δ given by the trace of the energy momentum tensor $\Theta^{\mu\mu}(T)$.

$$\frac{\Delta}{T^4} = \frac{\Theta^{\mu\mu}}{T^4} = \frac{\epsilon - 3p}{T^4} \quad (29)$$

In Fig. (3), we have plotted these thermodynamic quantities as obtained in PQMVT for both the parameter sets, ModelWB and ModelHotQCD with $\mathcal{U}_{\text{Poly-VM}}$ as the Polyakov loop potential. We have also plotted the PQM results

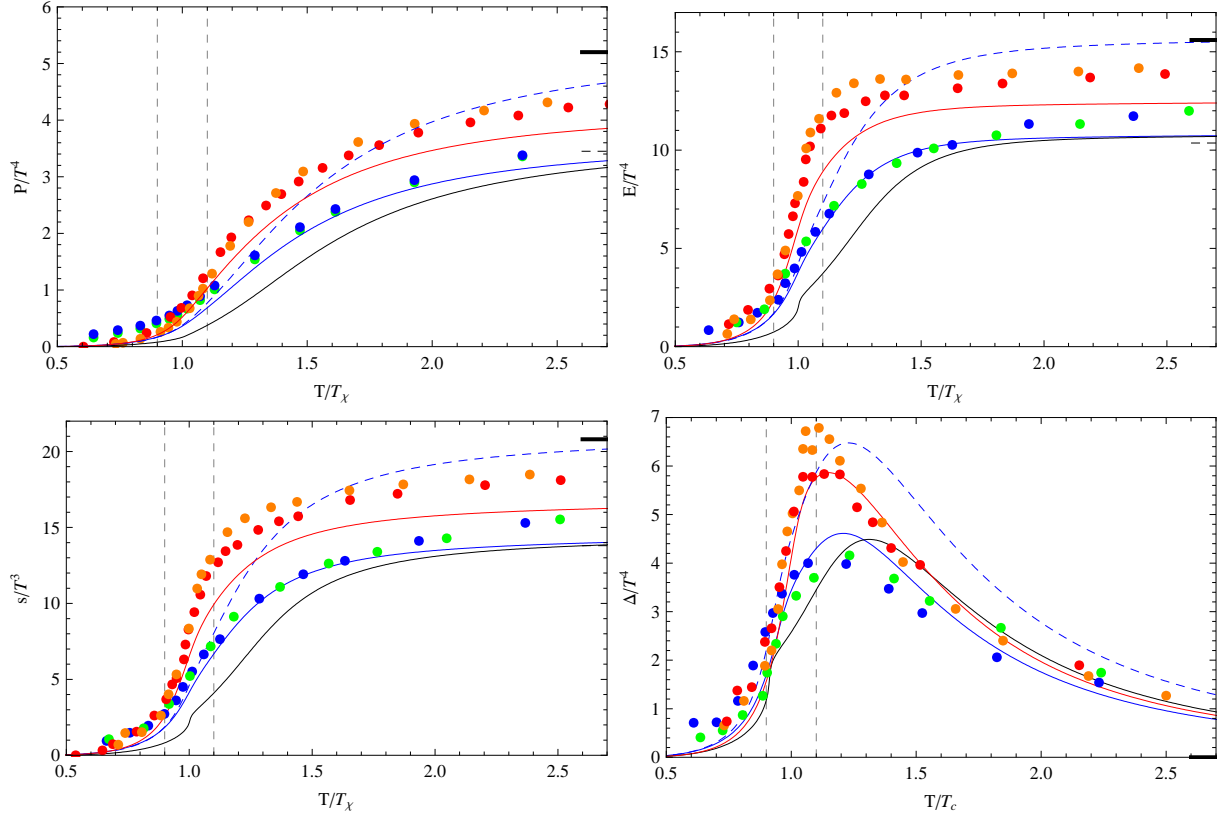


Figure 3: Plots of p , ϵ , s and Δ in PQMVT with ModelWB (blue solid) and ModelHotQCD (red solid) parameter sets. The corresponding black curves are the PQM predictions with ModelWB parameter set. These are obtained with the Polyakov potential $\mathcal{U}_{\text{Poly-VM}}$. For comparison, model predictions with the Polyakov potential $\mathcal{U}_{\text{Poly}}$ and ModelWB parameter set are also shown in dashed blue in each case. Here $T_c = \frac{T_x + T_d}{2}$. The LQCD data from WB are plotted in green and blue while the HotQCD data are plotted in orange and red. In case of p , the continuum estimate in blue and $N_\tau = 10$ WB data in green [44] are shown. Also shown are the $N_\tau = 8$ (red) [43] and $N_\tau = 6$ (orange) [42] HotQCD data. For both ϵ and s , LQCD data from WB are shown for $N_\tau = 10$ (blue) and $N_\tau = 8$ (green) [44] and HotQCD $N_\tau = 8$ [43] (red) and $N_\tau = 6$ [42] data are also shown. For Δ , WB data of continuum estimate [44] in blue and $N_\tau = 10$ [46] in green are shown while HotQCD $N_\tau = 8$ data with p4 (orange) and asqtad (red) [43] actions are also shown. In all the curves the high T SB limit of an ideal gas of massless fermions and gluons as in (30) is indicated by a thick black line while the dashed black line indicates the SB limit of an ideal gas of fermions only as in (30) without the first term.

with $\mathcal{U}_{\text{Poly-VM}}$ and PQMVT results with $\mathcal{U}_{\text{Poly}}$ for comparison. We find good qualitative agreement overall with LQCD. The smooth rise of p , ϵ and s with T for model as well as LQCD indicate the crossover nature of the phase transition that takes place at $\mu = 0$ [28, 38–41]. At low T , we see that Φ and $\bar{\Phi} \simeq 0$ and so it is clear from (17) that most of the contribution to thermodynamic quantities like p , ϵ and s come from the three-quark “hadron” states. This is how statistical confinement works generically in these model studies [48]. As is evident from Fig. (1), high values of σ_x and σ_y result in large mass for these effective degrees of freedom yielding suppressed values for all these thermodynamic quantities at lower temperatures. At larger temperatures, the melting of the quark condensates across T_χ (see Fig. (1)) result in lighter effective degrees of freedom. Also, Φ and $\bar{\Phi} \rightarrow 1$ resulting in the release of color states as the single quark states become the dominant degrees of freedom. This is manifested by all the three thermodynamic quantities that steadily rise across T_χ and saturate to a much higher value close to that of an ideal gas of N_f massless fermions and $(N_c^2 - 1)$ gluons whose pressure p_{SB} is given by

$$\frac{p_{SB}}{T^4} = (N_c^2 - 1) \frac{\pi^2}{45} + N_c N_f \frac{7\pi^2}{180}. \quad (30)$$

There is good agreement between ModelWB predictions for p , ϵ and s with the corresponding WB $N_\tau = 8, 10$ and continuum estimate [44] data in the temperature range $\approx 0.8 - 2 T_\chi$. At lower temperatures the agreement between model predictions and LQCD is not good which could be due to the mean field treatment of the mesons. Comparison of LQCD data with model predictions after taking into account mesonic fluctuations [49] should be carried out in order to throw more light on this issue. At higher temperatures the model description may not match well with LQCD as the contribution from the transverse gluons become significant and their physics may not be captured by the Polyakov loop Φ . The ModelHotQCD prediction although qualitatively in agreement with LQCD, lies slightly below the HotQCD data for all temperatures. However, it should be noted that the $N_\tau = 8$ data [43] is consistently lower than that of $N_\tau = 6$ [42] and so we expect that the agreement will improve when the continuum estimates will be available.

The model predictions for the conformal symmetry breaking measure Δ has also been plotted and compared with LQCD. In this case we have plotted Δ against $T_c = \frac{T_\chi + T_d}{2}$ for better agreement between model and LQCD. While for lower and higher temperatures, HotQCD [43] and WB [44, 46] data look reasonably consistent, around $1 - 1.5 T_c$ although both exhibit a peak, the height of the peak in case of HotQCD is almost 50% greater than that of WB. Moreover, the $N_\tau = 8$ HotQCD data with asqtad action is significantly lower than that of p4 action at the peak. Thus the LQCD prediction in this temperature regime is highly sensitive to the lattice volume as well as the lattice action implemented. As mentioned earlier, we have chosen the value of κ in (8) such that the model prediction agrees well with LQCD. In general κ could be taken as a function of T but in this work we have taken a constant value for κ .

The bumpy structures in $\langle \sigma_y \rangle$ and $\langle \Phi \rangle$ that we found around T_χ in Fig. 1 in the case of PQM shows up in the thermodynamic quantities also. Although the pressure looks smooth across the transition region, others like the ϵ , s and Δ which are functions of $\frac{\partial \Omega}{\partial T}$ exhibit bumps around T_χ . As observed in Fig. (1), addition of the vacuum term in PQMVT results in a smooth behaviour of the condensates in the transition region which in turn smoothens all the thermodynamic quantities in Fig. (3).

Another important quantity from the point of view of hydrodynamical investigations of relativistic heavy ion collisions is the isentropic speed of sound c_s given by

$$c_s^2 = \left. \frac{\partial p}{\partial \epsilon} \right|_s = \left. \frac{\partial p}{\partial T} \right|_V \bigg/ \left. \frac{\partial \epsilon}{\partial T} \right|_V = \frac{s}{c_V} \quad (31)$$

where c_V is the specific heat capacity at constant volume obtained as follows

$$c_V = \left. \frac{\partial \epsilon}{\partial T} \right|_V = -T \left. \frac{\partial^2 \Omega}{\partial T^2} \right|_V \quad (32)$$

c_s^2 is also closely related to the equation of state parameter p/ϵ [43]

$$c_s^2 = \frac{\partial p}{\partial \epsilon} = \epsilon \frac{\partial}{\partial \epsilon} \left(\frac{p}{\epsilon} \right) + \left(\frac{p}{\epsilon} \right) \quad (33)$$

In Fig. 4 we have plotted the model prediction for c_s^2 and p/ϵ against T and also ϵ . In the latter case the uncertainties due to T_χ go away. In Fig. 5 we have plotted the model prediction for c_v . The bumpy structures seen in Fig. 3 for

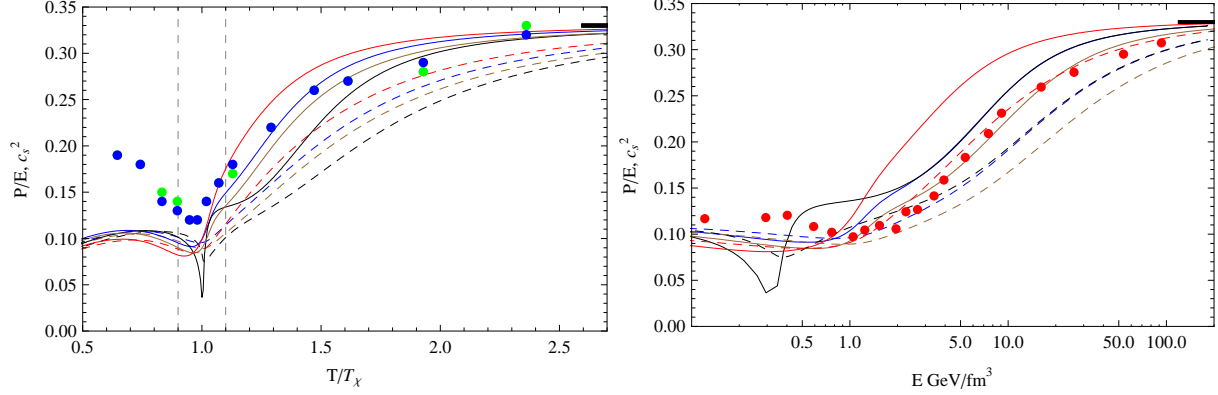


Figure 4: Plots of c_s^2 (solid) and p/ϵ (dashed) are shown in PQMVT with ModelWB (blue) and ModelHotQCD (red) parameter sets. The corresponding black curves are the PQM predictions with ModelWB parameter set. These are obtained with the Polyakov potential $\mathcal{U}_{\text{Poly-VM}}$. Also shown are the plots with $\mathcal{U}_{\text{Poly}}$ with ModelWB parameter set in brown for comparison. WB data of c_s^2 for $N_\tau = 10$ in green and the continuum estimate in blue [44] are shown. Also shown are the HotQCD $N_\tau = 8$ data [43] of p/ϵ in red. In all the curves the SB limit is indicated by a thick black line.

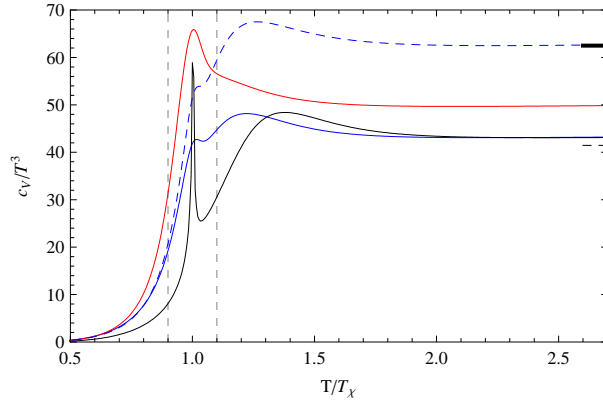


Figure 5: Plots of c_V in PQMVT with ModelWB (blue) and ModelHotQCD (red) are shown. The black curve is the PQM prediction with ModelWB parameter set. These are obtained with the Polyakov potential $\mathcal{U}_{\text{Poly-VM}}$. Also shown is the plot with $\mathcal{U}_{\text{Poly}}$ with ModelWB parameter set (blue dashed) for comparison. The high T SB limit of an ideal gas of massless fermions and gluons as in (30) is indicated by a thick black line while the dashed black line indicates the SB limit of an ideal gas of fermions only as in (30) without the first term.

PQM becomes even more prominent in c_s^2 and c_V which depend on $\frac{\partial^2 \Omega}{\partial T^2}$. c_V exhibits a sharp spike like structure at T_χ which results in a sharp dip in c_s^2 at the same temperature. The PQMVT plots are lot smoother and compare well with LQCD qualitatively. Around T_χ , WB continuum estimate for c_s^2 [44] show a minimum with a value around 0.12 while ModelWB also exhibits a minimum in the same region with a minimum value ~ 0.08 . In the high T limit, both c_s^2 and p/ϵ for model and LQCD are found to approach the SB limit $1/3$. In case of c_V the high temperature limit is dependent on the Polyakov potential chosen. As seen in Fig. (5), the model prediction with $\mathcal{U}_{\text{Poly}}$ saturates to the SB limit by $2T_\chi$ whereas the model prediction with $\mathcal{U}_{\text{Poly-VM}}$ saturates to a lower value $\sim 73\%$ of the SB limit. Similarly even in the case of p , ϵ and s in the high temperature we find the model predictions with $\mathcal{U}_{\text{Poly-VM}}$ always lower than those with $\mathcal{U}_{\text{Poly}}$.

We end this subsection with an interesting observation. We find that the model prediction for the thermodynamic quantities like p , ϵ , s and c_V with ModelWB parameter set and $\mathcal{U}_{\text{Poly-VM}}$ Polyakov potential for high temperatures saturate close to the SB limit of an ideal gas with only massless fermions and no gluons which is the p_{SB} from (30) after removing the first term due to gluons. In [28] similar results were reported when the Fukushima ansatz [50] for the Polyakov potential was used. Thus we find that the high temperature behaviour for model predictions with ModelWB parameter set and $\mathcal{U}_{\text{Poly-VM}}$ is similar to that of the Fukushima potential [50] which is based on a strong coupling analysis.

3.2 Quark Number Susceptibilities

Quark number susceptibilities (QNS) are defined as derivatives of pressure with respect to quark chemical potentials

$$\chi_{ijk}^{uds} = \frac{\partial^{i+j+k}(p/T^4)}{\partial(\mu_u/T)^i \partial(\mu_d/T)^j \partial(\mu_s/T)^k} \quad (34)$$

Linear combinations of these can be related to fluctuations and correlations of conserved charges like baryon number, electric charge and strangeness which have been proposed as possible observables to signal the QCD phase transition [54, 55]. These have been measured in LQCD [43, 45, 47, 51–53]. Here we show results on QNS upto second order. A detailed analysis of the fluctuations and correlations of conserved charges in PQMVT and their comparison with LQCD will be done elsewhere [56].

Fig. (6) shows the diagonal susceptibilities χ_2^u and χ_2^s , their ratio χ_2^s/χ_2^u and the off-diagonal χ_2^{us} . All susceptibilities vanish at low temperature since the condensates have large values which implies large masses of the relevant degrees of freedom that restricts the capacity of fluctuations. At high temperature where the degrees of freedom have small masses and temperature is the only relevant scale, the system begins to behave like an ideal gas of massless quarks. The susceptibilities thus approach the corresponding SB limit of ideal gas of three quarks.

The diagonal susceptibilities both show a monotonic increase with temperature, with the maximum rate of increase observed around the crossover region and then saturating at higher temperatures to the SB limit. Both χ_2^u and χ_2^s saturate to about 80 – 90% of the SB limit at $T \sim 2.4T_\chi$. We also observe that the light quark susceptibility rises much faster than that of the strange quark both in model as well as LQCD. χ_2^s begins to saturate well beyond the cross-over region as is expected from the slow decrease of the value of the strange condensate. For both χ_2^u and χ_2^s the $N_\tau = 8$ data with asqtad action for HotQCD [43] lie consistently above ModelHotQCD. On the other hand, there is much better agreement between WB data and ModelWB predictions. It is interesting to observe that the recent $N_\tau = 8$ susceptibility data with hisq action from HotQCD [47] which has also been plotted in Fig. (6) agree much better with the WB data.

It is useful to consider the ratio of the two susceptibilities, χ_2^s/χ_2^u , in order to avoid unknown normalization factors that maybe present in lattice data [16, 52]. In the unbroken phase there is excellent agreement between the models and lattice data, but they do not match as well below the crossover temperature. This maybe attributed to absence of mesonic fluctuations in a mean field approximation calculation [28]. However, this ratio in the low temperature region is also highly dependent on the form of the Polyakov potential (see Fig. (6 b) of [28]). In our case the potential we use improves marginally the agreement of the model to lattice predictions by giving smaller values to this ratio in the low temperature region. It should also be noted that the lattice data in this region have large errors and comparisons of the model to lattice are uncertain.

We also show in Fig. (6) the off-diagonal susceptibility χ_2^{us} , which represents the correlation between the light and heavy quarks. It vanishes in the SB limit, as is expected for a non-interacting ideal gas, and peaks in the crossover region. Qualitatively the χ_2^{us} predictions of the model agree with lattice, showing the same essential features, however,

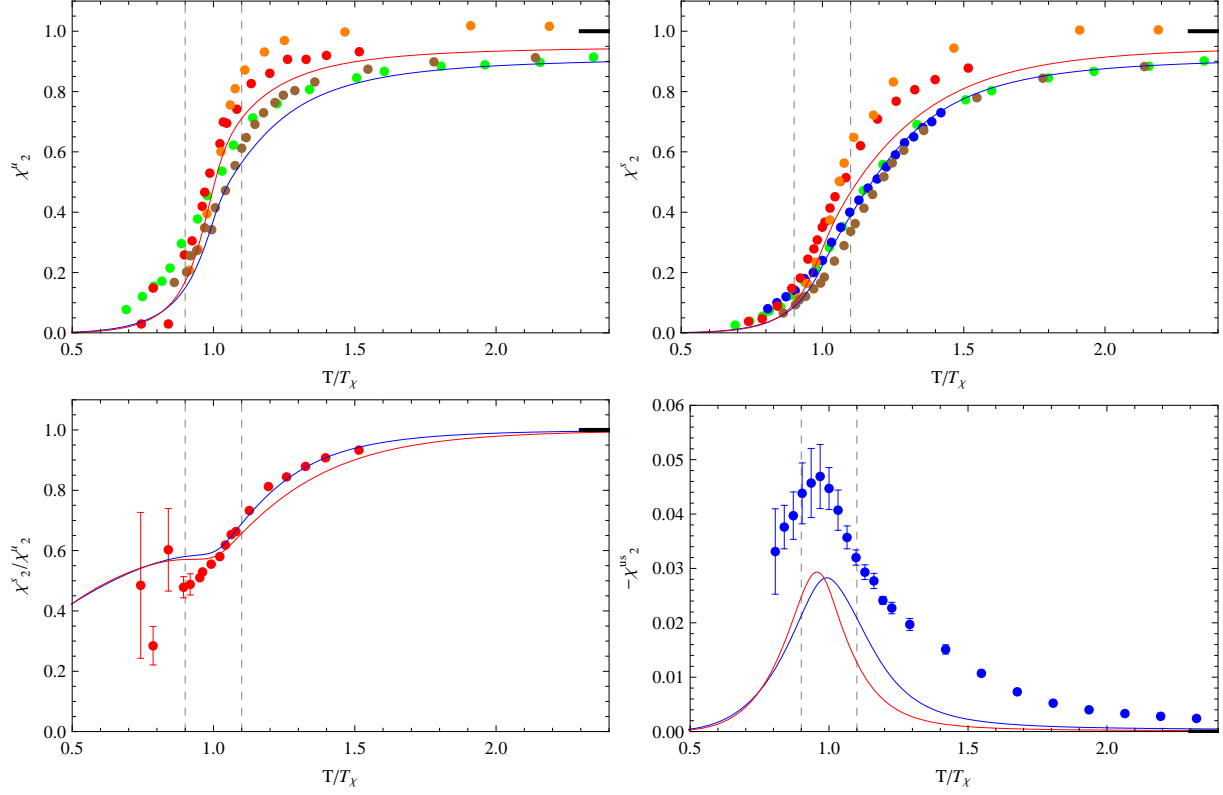


Figure 6: QNS as obtained in PQMVT are plotted for ModelWB (blue) and ModelHotQCD (red) with the Polyakov potential $\mathcal{U}_{\text{Poly-V}}^{\text{M}}$. For both χ_2^μ and χ_2^s , WB $N_\tau = 12$ data [51] (green) and HotQCD $N_\tau = 8$ [43] (red), $N_\tau = 6$ [52] (orange) and $N_\tau = 8$ with hisq action [47] (brown) are shown for comparison. Also in case of χ_2^s , WB continuum estimate [45] is shown in blue. The HotQCD data for χ_2^s/χ_2^μ in red [43] and the WB continuum estimate for χ_2^{us} [53] in blue are also compared with the model predictions. The high T SB limit is indicated by a thick black line.

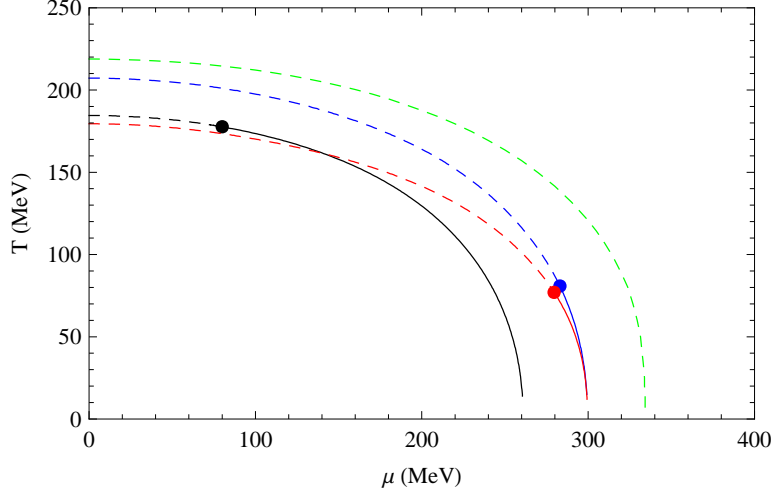


Figure 7: Phase diagrams for PQM (black) in ModelWB and PQMVT in ModelWB (blue) and ModelHotQCD (red) with the Polyakov potential $\mathcal{U}_{\text{Poly-VM}}$. The dashed lines indicate crossover, the solid lines indicate first order phase transition and the filled circles indicate CEP. The phase diagram for $m_\sigma = 600$ MeV in the case of PQMVT with the Polyakov potential $\mathcal{U}_{\text{Poly}}$ is also shown (green).

lattice data is consistently larger over the entire temperature range. This maybe due to unknown normalization factors of lattice and perhaps a better quantity to compare would be normalized correlations [56].

3.3 Phase Diagram

The divergence of χ_2^u can be used to locate the CEP [57] where a first order phase transition line ends in a second order phase transition point. We obtain the phase diagram in the case of symmetric quark matter ($\mu_x = \mu_y = \mu$). In Fig. (7) we have presented the phase diagram for PQM and PQMVT. The chiral phase boundary has been plotted and the CEP located in all the cases. The smoothening of the thermodynamic quantities in the transition region as seen for $\mu = 0$ persists even at non-zero chemical potentials. This results in pushing the CEP to a higher value of μ in case of PQMVT as compared to PQM. With $m_\sigma = 400$ MeV, in PQM with ModelWB using the $\mathcal{U}_{\text{Poly-VM}}$ potential the CEP is found at $(\mu, T) = (80, 177.5)$ MeV which gets shifted to $(283, 81)$ MeV in case of PQMVT of ModelWB. We have also obtained the phase diagram in PQMVT with $m_\sigma = 600$ MeV and $\mathcal{U}_{\text{Poly}}$ potential. In this case the phase diagram has no CEP and there is only crossover transition on the entire $(\mu - T)$ plane as in the case of 2 flavors [26].

We have also plotted the phase boundary of PQMVT in ModelHotQCD (red) with the $\mathcal{U}_{\text{Poly-VM}}$ potential. In this case T_χ is lower than that of ModelWB at $\mu = 0$ that result in a lower phase boundary in the (T, μ) plane as compared to the case with ModelWB parameter set. This is the effect of choosing a smaller value of T_0 . For large values of μ there is not much difference between the two phase boundaries. This is essentially because in this region the Polyakov potential plays a less important role as compared to $\Omega_{q\bar{q}}$. The phase boundary for ModelWB with $\mathcal{U}_{\text{Poly}}$ does not differ much from that of ModelWB with the $\mathcal{U}_{\text{Poly-VM}}$ potential implying that in this case the VanderMonde term does not play much of a role in the determination of the chiral phase boundary.

4 Conclusion

In this paper we have studied the effect of including the commonly neglected fermionic vacuum fluctuations to the $(2+1)$ PQM model. The conventional PQM model suffers from a rapid phase transition contrary to what is found through lattice simulations [28]. This could be due to the use of a Polyakov potential which carries with it a remnant first order phase transition of the pure glue theory. Another possible reason could be the sudden release of quark degrees of freedom in PQM with increase in temperature. Addition of the vacuum term in PQMVT addresses the latter.

This tames the rapid transitions that we see in the PQM model and significantly improves the model's agreement to lattice data.

We work with two Polyakov loop potentials: $\mathcal{U}_{\text{Poly}}$ and $\mathcal{U}_{\text{Poly-VM}}$ given in (7) and (8) respectively. The model parameters are fixed by inputs from experiments as well as LQCD data. In this work, we have compared model predictions to LQCD data of HotQCD and WB groups. Depending on the lattice group whose data we choose to fix the model parameters, we arrive at the two sets of model parameters namely ModelWB and ModelHotQCD given in Table 1. We then investigated the bulk thermodynamic properties of the system and the influence of the vacuum term in PQMVT. In PQM, $\Delta_{l,s}$ which is a suitably defined order parameter for chiral phase transition is found to undergo a much rapid fall across the transition temperatures compared to LQCD [28]. The inclusion of the fermionic vacuum fluctuations in the model makes the transition much more gentle. The vacuum term essentially washes away all the jagged and bumpy structures that are there in the quark condensates, Polyakov loop and all thermodynamic quantities in PQM. We also computed the QNS upto second order. In all cases very good qualitative agreement between LQCD and model is found. The model computations suggest that the high temperature behaviour of the thermodynamic quantities with $\mathcal{U}_{\text{Poly-VM}}$ Polyakov potential and ModelWB parameter set is similar to that of the Fukushima potential [50] for the Polyakov loop. We further investigated the role of the vacuum term on the phase diagram. The smoothening effect of the vacuum term persists even at non zero μ . With $m_\sigma = 600$ MeV, we find that the vacuum term washes away the critical behaviour completely from the (μ, T) plane. In case of $m_\sigma = 400$ MeV, addition of the vacuum term pushes the CEP to larger chemical potential.

5 Acknowledgement

S.C. would like to acknowledge discussions and collaborations with Sourendu Gupta for introduction to the subject itself. He would also like to acknowledge many helpful discussions with Uma Shankar Gupta, Anirban Lahiri, Tanumoy Mandal, Apoorva Patel and Rajarshi Ray. We would like to thank Rohini Godbole for guidance. K.A.M. acknowledges the financial support through Junior Research Fellowship provided by CSIR.

6 Appendix

A Model Parameters

The model parameters are determined by establishing the vacuum properties. In analogy to [15,32] the values of the condensates are determined from the pion and kaon decay constants by means of the partially conserved axial-vector current relation (PCAC). In the strange-non-strange basis they are given by

$$\bar{\sigma}_x = f_\pi ; \quad \bar{\sigma}_y = \frac{1}{\sqrt{2}}(2f_K - f_\pi) . \quad (35)$$

The remaining model parameters (m^2 , λ_1 , λ_2 , c , h_x and h_y) are fixed by the following inputs from experiments: pion mass m_π and pion decay constant f_π , kaon mass m_K and kaon decay constant f_K , average squared mass of η and η' mesons, $(m_\eta^2 + m_{\eta'}^2)$ and sigma mass m_σ . In this appendix we shall derive the equations to determine the above parameters in PQMVT.

Using (10) and (14), we rewrite $\Omega(T, \mu_x, \mu_y)$ as

$$\Omega^{\text{PQMVT}}(T, \mu_x, \mu_y) = \Omega^{\text{PQM}}(T, \mu_x, \mu_y) + \Omega_{\bar{q}q}^v \quad (36)$$

where

$$\Omega^{\text{PQM}}(T, \mu_x, \mu_y) = U(\sigma_x, \sigma_y) + \mathcal{U}_P(\Phi, \bar{\Phi}, T) + \Omega_{\bar{q}q}^{th} \quad (37)$$

| Mesons | Expression for masses |
|--|--|
| m_π^2 | $m^2 + \lambda_1(x^2 + y^2) + \frac{\lambda_2}{2}x^2 - \frac{\sqrt{2}c}{2}y - \frac{N_c g^4}{64\pi^2}x^2 X$ |
| m_K^2 | $m^2 + \lambda_1(x^2 + y^2) + \frac{\lambda_2}{2}(x^2 - \sqrt{2}xy + 2y^2) - \frac{c}{2}x - \frac{N_c g^4}{64\pi^2}\left(\frac{x - \sqrt{2}y}{x^2 - 2y^2}\right)(x^3 X + 2\sqrt{2}y^3 Y)$ |
| $m_{p,00}^2$ | $m^2 + \lambda_1(x^2 + y^2) + \frac{\lambda_2}{3}(x^2 + y^2) + \frac{c}{3}(2x + \sqrt{2}y) - \frac{N_c g^4}{96\pi^2}(x^2 X + y^2 Y)$ |
| $m_{p,88}^2$ ($m_\eta^2 + m_{\eta'}^2$) | $m^2 + \lambda_1(x^2 + y^2) + \frac{\lambda_2}{6}(x^2 + 4y^2) - \frac{c}{6}(4x - \sqrt{2}y) - \frac{N_c g^4}{192\pi^2}(x^2 X + 4y^2 Y)$ $m_{p,00}^2 + m_{p,88}^2$ |
| $m_{s,00}^2$ | $m^2 + \frac{\lambda_1}{3}(7x^2 + 4\sqrt{2}xy + 5y^2) + \lambda_2(x^2 + y^2) - \frac{\sqrt{2}c}{3}(\sqrt{2}x + y) - \frac{N_c g^4}{96\pi^2}(3(x^2 X + y^2 Y) + 4(x^2 + y^2))$ |
| $m_{s,88}^2$ | $m^2 + \frac{\lambda_1}{3}(5x^2 - 4\sqrt{2}xy + 7y^2) + \lambda_2(\frac{x^2}{2} + 2y^2) + \frac{\sqrt{2}c}{3}(\sqrt{2}x - \frac{y}{2}) - \frac{N_c g^4}{96\pi^2}(\frac{3}{2}(x^2 X + 4y^2 Y) + 2(x^2 + 4y^2))$ |
| $m_{s,08}^2$ | $\frac{2\lambda_1}{3}(\sqrt{2}x^2 - xy - \sqrt{2}y^2) + \sqrt{2}\lambda_2(\frac{x^2}{2} - y^2) + \frac{c}{3\sqrt{2}}(x - \sqrt{2}y) - \frac{N_c g^4}{8\sqrt{2}\pi^2}(\frac{1}{4}(x^2 X - 2y^2 Y) + \frac{1}{3}(x^2 - 2y^2))$ |
| m_σ^2 | $m_{s,00}^2 \cos^2 \theta_s + m_{s,88}^2 \sin^2 \theta_s + 2m_{s,08}^2 \sin \theta_s \cos \theta_s$, where $\tan(2\theta_s) = \frac{2m_{s,08}^2}{m_{s,00}^2 - m_{s,88}^2}$ |

Table 2: The expressions of squared meson masses in the vacuum required to determine the model parameters. x denotes σ_x , y denotes σ_y , X denotes $(1 + 4 \log(\frac{g\sigma_x}{2\Lambda}))$ and Y denotes $(1 + 4 \log(\frac{g\sigma_y}{\sqrt{2}\Lambda}))$.

Now the meson masses are determined by the curvature of Ω at the global minimum

$$\begin{aligned}
m_{\alpha,ab}^2 &= \left. \frac{\partial^2 \Omega}{\partial \xi_{\alpha,a} \partial \xi_{\alpha,b}} \right|_{\min} \\
&= \left. \frac{\partial^2 \Omega^{\text{PQM}}}{\partial \xi_{\alpha,a} \partial \xi_{\alpha,b}} \right|_{\min} + \left. \frac{\partial^2 \Omega_{qq}^v}{\partial \xi_{\alpha,a} \partial \xi_{\alpha,b}} \right|_{\min} \\
&= m_{\alpha,ab}^{\text{PQM}^2} + m_{\alpha,ab}^{v^2}
\end{aligned} \tag{38}$$

$m_{\alpha,ab}^{\text{PQM}^2}$ are available in the literature [32]. Here we compute $m_{\alpha,ab}^{v^2}$. From (19) and (38) we get

$$m_{\alpha,ab}^{v^2} = -\frac{N_c}{8\pi^2} \sum_f \left[\left(2 \log\left(\frac{m_f}{\Lambda}\right) + \frac{3}{2} \right) \left(\frac{\partial m_f^2}{\partial \xi_{\alpha,a}^2} \right) \left(\frac{\partial m_f^2}{\partial \xi_{\alpha,b}^2} \right) + \left(\frac{m_f^2}{2} + 2m_f^2 \log\left(\frac{m_f}{\Lambda}\right) \right) \frac{\partial^2 m_f^2}{\partial \xi_{\alpha,a} \partial \xi_{\alpha,b}} \right] \tag{39}$$

The expressions for $\left(\frac{\partial m_f^2}{\partial \xi_{\alpha,a}}\right)$, $\left(\frac{\partial m_f^2}{\partial \xi_{\alpha,b}}\right)$ and $\frac{\partial^2 m_f^2}{\partial \xi_{\alpha,a} \partial \xi_{\alpha,b}}$ are already available in [32]. In Table (2), we present the expressions of $m_{\alpha,ab}^2$ for the different mesons as obtained in PQMVT at $T = \mu = 0$.

From the expressions of m_π^2 , m_K^2 and $(m_\eta^2 + m_{\eta'}^2)$ we find λ_2 and c

$$\begin{aligned}
\lambda_2 &= \frac{3(2f_K - f_\pi)m_K'^2 - (2f_K + f_\pi)m_\pi'^2 - 2(m_\eta^2 + m_{\eta'}^2)'(f_K - f_\pi)}{(3f_\pi^2 + 8f_K(f_K - f_\pi))(f_K - f_\pi)} \\
c &= \frac{m_K'^2 - m_\pi'^2}{f_K - f_\pi} - \lambda_2(2f_K - f_\pi)
\end{aligned} \tag{40}$$

where

$$\begin{aligned}
m_K'^2 &= m_K^2 + \frac{N_c g^4}{64\pi^2} \left(\frac{x - \sqrt{2}y}{x^2 - 2y^2} \right) (x^3 X + 2\sqrt{2}y^3 Y) \\
m_\pi'^2 &= m_\pi^2 + \frac{N_c g^4}{64\pi^2} x^2 X \\
(m_\eta^2 + m_{\eta'}^2)' &= (m_\eta^2 + m_{\eta'}^2) + \frac{N_c g^4}{96\pi^2} (x^2 X + y^2 Y) + \frac{N_c g^4}{192\pi^2} (x^2 X + 4y^2 Y)
\end{aligned} \tag{41}$$

Here x denotes σ_x , y denotes σ_y , X denotes $(1 + 4 \log(\frac{g\sigma_x}{2\Lambda}))$ and Y denotes $(1 + 4 \log(\frac{g\sigma_y}{\sqrt{2}\Lambda}))$. Having obtained λ_2

and c , we use the expression of m_π^2 to express m^2 in terms of λ_1

$$m^2 = m_\pi'^2 - \frac{\lambda_2}{2} f_\pi^2 + \frac{c}{2} (2f_K - f_\pi) - \lambda_1 \left(f_\pi^2 + \frac{(2f_K - f_\pi)^2}{2} \right) \quad (42)$$

Finally, λ_1 may be obtained from the expression of m_σ^2 while the explicit symmetry breaking parameters h_x and h_y are obtained from the stationarity conditions (20)

$$h_x = f_\pi m_\pi'^2 - \frac{N_c g^4 \sigma_x^3}{64\pi^2} \left(1 + 4 \log \left(\frac{g\sigma_x}{2\Lambda} \right) \right) \quad (43)$$

$$h_y = \sqrt{2} f_K m_K'^2 - \frac{f_\pi m_\pi'^2}{\sqrt{2}} - \frac{N_c g^4 \sigma_y^3}{32\pi^2} \left(1 + 4 \log \left(\frac{g\sigma_y}{\sqrt{2}\Lambda} \right) \right) \quad (44)$$

Thus the final expression of the parameters are

$$\begin{aligned}
h_x &= f_\pi m_\pi^2; \\
h_y &= \frac{2f_K m_K^2 - f_\pi m_\pi^2}{\sqrt{2}}; \\
\lambda_2(\Lambda) &= \left(g^4 \text{Log} \left[\frac{gf_\pi}{2\Lambda} \right] f_\pi^2 (-8f_K^2 + 8f_K f_\pi - 3f_\pi^2) N_c + \right. \\
&\quad g^4 \text{Log} \left[\frac{g(2f_K - f_\pi)}{2\Lambda} \right] (-2f_K + f_\pi)^2 (8f_K^2 - 8f_K f_\pi + 3f_\pi^2) N_c + \\
&\quad f_K (8g^4 f_K^3 N_c - 16g^4 f_K^2 f_\pi N_c - f_\pi (32\pi^2 (3m_K^2 + m_\pi^2 - 2(m_\eta^2 + m_{\eta'}^2)) + 3g^4 f_\pi^2 N_c) + \\
&\quad f_K (-64\pi^2 (-3m_K^2 + m_\pi^2 + m_\eta^2 + m_{\eta'}^2) + 11g^4 f_\pi^2 N_c)) / (32\pi^2 f_K (8f_K^3 - 16f_K^2 f_\pi + 11f_K f_\pi^2 - 3f_\pi^3)) \Big); \\
c &= -\frac{2(2f_K(m_K^2 + m_\pi^2 - m_\eta^2 - m_{\eta'}^2) + f_\pi(-2m_\pi^2 + m_\eta^2 + m_{\eta'}^2))}{8f_K^2 - 8f_K f_\pi + 3f_\pi^2}; \\
m^2 &= \left(-g^4 \text{Log} \left[\frac{(2f_K - f_\pi)}{f_\pi} \right] f_\pi^2 (-2f_K + f_\pi)^2 (8f_K^2 - 8f_K f_\pi + 3f_\pi^2) N_c - \right. \\
&\quad 32\pi^2 f_K (32f_K^5 \lambda_1 - 96f_K^4 f_\pi \lambda_1 + f_\pi^3 (-3m_K^2 + m_\pi^2 + 4(m_\eta^2 + m_{\eta'}^2) - 9f_\pi^2 \lambda_1) - \\
&\quad 4f_K^2 f_\pi (3m_K^2 - 3m_\pi^2 - 4(m_\eta^2 + m_{\eta'}^2) + 26f_\pi^2 \lambda_1) + 4f_K^3 (-2(-m_K^2 + m_\pi^2 + m_\eta^2 + m_{\eta'}^2) + 33f_\pi^2 \lambda_1) + \\
&\quad f_K f_\pi^2 (10m_K^2 - 8m_\pi^2 - 12(m_\eta^2 + m_{\eta'}^2) + 45f_\pi^2 \lambda_1)) / (64\pi^2 f_K (8f_K^3 - 16f_K^2 f_\pi + 11f_K f_\pi^2 - 3f_\pi^3)) \Big); \\
m_\sigma^2 &= m_{s,00}^2 \cos^2 \theta_s + m_{s,88}^2 \sin^2 \theta_s + 2m_{s,08}^2 \sin \theta_s \cos \theta_s, \quad \text{where} \\
m_{s,00}^2 &= \left(3g^4 \text{Log} \left[\frac{(2f_K - f_\pi)}{f_\pi} \right] f_\pi^2 (-2f_K + f_\pi)^2 (8f_K^2 - 8f_K f_\pi + 3f_\pi^2) N_c - \right. \\
&\quad 2f_K (32f_K^5 (g^4 N_c - 16\pi^2 \lambda_1) + f_K^4 f_\pi (-96g^4 N_c + 512\pi^2 \lambda_1) + \\
&\quad f_K f_\pi^2 (16\pi^2 (-26m_K^2 - 9m_\pi^2 + m_\eta^2 + m_{\eta'}^2) + f_\pi^2 (45g^4 N_c + 16\pi^2 \lambda_1)) - \\
&\quad 8f_K^2 f_\pi (16\pi^2 (-5m_K^2 - 3m_\pi^2 + m_\eta^2 + m_{\eta'}^2) + f_\pi^2 (13g^4 N_c + 32\pi^2 \lambda_1)) + \\
&\quad f_\pi^3 (-16\pi^2 (-9m_K^2 - 2m_\pi^2 + m_\eta^2 + m_{\eta'}^2) + f_\pi^2 (-9g^4 N_c + 48\pi^2 \lambda_1)) + \\
&\quad 4f_K^3 (32\pi^2 (-4m_K^2 - m_\pi^2 + m_\eta^2 + m_{\eta'}^2) + f_\pi^2 (33g^4 N_c + 48\pi^2 \lambda_1))) / (96\pi^2 f_K (8f_K^3 - 16f_K^2 f_\pi + \\
&\quad 11f_K f_\pi^2 - 3f_\pi^3)) \Big); \\
m_{s,88}^2 &= \left(3g^4 \text{Log} \left[\frac{(2f_K - f_\pi)}{f_\pi} \right] f_\pi^2 (-2f_K + f_\pi)^2 (8f_K^2 - 8f_K f_\pi + 3f_\pi^2) N_c - \right. \\
&\quad 2f_K (-64f_K^4 f_\pi (3g^4 N_c - 64\pi^2 \lambda_1) + 64f_K^5 (g^4 N_c - 16\pi^2 \lambda_1) + \\
&\quad f_K f_\pi^2 (16\pi^2 (-58m_K^2 - 39m_\pi^2 + 32(m_\eta^2 + m_{\eta'}^2)) + f_\pi^2 (57g^4 N_c - 2176\pi^2 \lambda_1)) - \\
&\quad 32f_K^2 f_\pi (4\pi^2 (-13m_K^2 - 3m_\pi^2 + 5(m_\eta^2 + m_{\eta'}^2)) + f_\pi^2 (5g^4 N_c - 164\pi^2 \lambda_1)) + \\
&\quad 16f_K^3 (8\pi^2 (-8m_K^2 + m_\pi^2 + 2(m_\eta^2 + m_{\eta'}^2)) + 3f_\pi^2 (5g^4 N_c - 136\pi^2 \lambda_1)) + \\
&\quad f_\pi^3 (16\pi^2 (9m_K^2 + 16m_\pi^2 - 8(m_\eta^2 + m_{\eta'}^2)) + \\
&\quad f_\pi^2 (-9g^4 N_c + 384\pi^2 \lambda_1))) / (96\pi^2 f_K (8f_K^3 - 16f_K^2 f_\pi + 11f_K f_\pi^2 - 3f_\pi^3)) \Big); \\
m_{s,08}^2 &= (8f_K^4 (g^4 N_c - 16\pi^2 \lambda_1) - 16f_K^3 f_\pi (g^4 N_c - 12\pi^2 \lambda_1) + 8\pi^2 f_\pi^2 (2m_\pi^2 - m_\eta^2 - m_{\eta'}^2 + 3f_\pi^2 \lambda_1) + \\
&\quad f_K^2 (32\pi^2 (-4m_K^2 + 2m_\pi^2 + m_\eta^2 + m_{\eta'}^2) + f_\pi^2 (11g^4 N_c - 48\pi^2 \lambda_1)) - \\
&\quad f_K f_\pi (8\pi^2 (-7m_K^2 + m_\pi^2 + 3(m_\eta^2 + m_{\eta'}^2)) + f_\pi^2 (3g^4 N_c + 40\pi^2 \lambda_1))) / (6\sqrt{2}\pi^2 (8f_K^2 - 8f_K f_\pi + 3f_\pi^2)); \\
\tan(2\theta_s) &= \frac{2m_{s,08}^2}{m_{s,00}^2 - m_{s,88}^2}; \tag{45}
\end{aligned}$$

Hence only λ_2 depends on Λ . It is straightforward but tedious to check that this dependence cancels neatly with that of $\Omega_{\bar{q}q}^v$ in (10) to yield a Λ independent Ω .

References

- [1] L. D. McLerran and B. Svetitsky, Phys. Rev. D **24** (1981) 450.
- [2] B. Svetitsky, Phys. Rept. **132** (1986) 1.
- [3] B. Muller, Rept. Prog. Phys. **58** (1995) 611 [nucl-th/9410005].
- [4] D. H. Rischke, Prog. Part. Nucl. Phys. **52** (2004) 197 [nucl-th/0305030].
- [5] K. Fukushima and T. Hatsuda, Rept. Prog. Phys. **74** (2011) 014001 [arXiv:1005.4814 [hep-ph]].
- [6] P. de Forcrand, PoS LAT **2009** (2009) 010 [arXiv:1005.0539 [hep-lat]].
- [7] S. Gupta, PoS LATTICE **2010** (2010) 007 [arXiv:1101.0109 [hep-lat]].
- [8] A. M. Polyakov, Phys. Lett. B **72** (1978) 477.
- [9] Y. Nambu and G. Jona-Lasinio, Phys. Rev. **122** (1961) 345.
- [10] Y. Nambu and G. Jona-Lasinio, Phys. Rev. **124** (1961) 246.
- [11] M. Asakawa and K. Yazaki, Nucl. Phys. A **504** (1989) 668.
- [12] T. Hatsuda and T. Kunihiro, Phys. Rev. Lett. **55** (1985) 158.
- [13] M. Gell-Mann and M. Levy, Nuovo Cim. **16** (1960) 705.
- [14] B.W. Lee, Chiral Dynamics, Gordon and Breach, New York, 1972.
- [15] J. T. Lenaghan, D. H. Rischke and J. Schaffner-Bielich, Phys. Rev. D **62** (2000) 085008 [nucl-th/0004006].
- [16] B. -J. Schaefer and M. Wagner, Phys. Rev. D **79** (2009) 014018 [arXiv:0808.1491 [hep-ph]].
- [17] P. N. Meisinger and M. C. Ogilvie, Phys. Lett. B **379** (1996) 163 [hep-lat/9512011].
- [18] K. Fukushima, Phys. Lett. B **591** (2004) 277 [hep-ph/0310121].
- [19] C. Ratti, M. A. Thaler and W. Weise, Phys. Rev. D **73** (2006) 014019 [hep-ph/0506234].
- [20] S. K. Ghosh, T. K. Mukherjee, M. G. Mustafa and R. Ray, Phys. Rev. D **73** (2006) 114007 [hep-ph/0603050].
- [21] B. -J. Schaefer, J. M. Pawłowski and J. Wambach, Phys. Rev. D **76** (2007) 074023 [arXiv:0704.3234 [hep-ph]].
- [22] H. Mao, J. Jin and M. Huang, J. Phys. G **37** (2010) 035001 [arXiv:0906.1324 [hep-ph]].
- [23] V. Skokov, B. Friman, E. Nakano, K. Redlich and B. -J. Schaefer, Phys. Rev. D **82** (2010) 034029 [arXiv:1005.3166 [hep-ph]].
- [24] E. Nakano, B. -J. Schaefer, B. Stokic, B. Friman and K. Redlich, Phys. Lett. B **682** (2010) 401 [arXiv:0907.1344 [hep-ph]].
- [25] A. J. Mizher, M. N. Chernodub and E. S. Fraga, Phys. Rev. D **82** (2010) 105016 [arXiv:1004.2712 [hep-ph]].
- [26] U. S. Gupta and V. K. Tiwari, Phys. Rev. D **85** (2012) 014010 [arXiv:1107.1312 [hep-ph]].
- [27] B. -J. Schaefer, M. Wagner and J. Wambach, PoS CPOD **2009** (2009) 017 [arXiv:0909.0289 [hep-ph]].
- [28] B. -J. Schaefer, M. Wagner and J. Wambach, Phys. Rev. D **81** (2010) 074013 [arXiv:0910.5628 [hep-ph]].
- [29] S. Roessner, C. Ratti and W. Weise, Phys. Rev. D **75** (2007) 034007 [hep-ph/0609281].
- [30] S. K. Ghosh, T. K. Mukherjee, M. G. Mustafa and R. Ray, Phys. Rev. D **77** (2008) 094024 [arXiv:0710.2790 [hep-ph]].

- [31] O. Scavenius, A. Mocsy, I. N. Mishustin and D. H. Rischke, Phys. Rev. C **64** (2001) 045202 [nucl-th/0007030].
- [32] B. -J. Schaefer and M. Wagner, Phys. Rev. D **79** (2009) 014018 [arXiv:0808.1491 [hep-ph]].
- [33] Finite Temperature Field Theory Principles and Applications, J. I. Kapusta and C. Gale, Cambridge University Press, Cambridge, England (2006).
- [34] K. Nakamura *et al.* [Particle Data Group Collaboration], J. Phys. G **37** (2010) 075021.
- [35] I. Caprini, G. Colangelo and H. Leutwyler, Phys. Rev. Lett. **96** (2006) 132001 [hep-ph/0512364].
- [36] J. Braun and H. Gies, Phys. Lett. B **645** (2007) 53 [hep-ph/0512085].
- [37] J. Braun and H. Gies, JHEP **0606** (2006) 024 [hep-ph/0602226].
- [38] Y. Aoki, G. Endrodi, Z. Fodor, S. D. Katz and K. K. Szabo, Nature **443** (2006) 675 [hep-lat/0611014].
- [39] M. Cheng, N. H. Christ, S. Datta, J. van der Heide, C. Jung, F. Karsch, O. Kaczmarek and E. Laermann *et al.*, Phys. Rev. D **74** (2006) 054507 [hep-lat/0608013].
- [40] S. Borsanyi, G. Endrodi, Z. Fodor, A. Jakovac, S. D. Katz, S. Krieg, C. Ratti and K. K. Szabo, arXiv:1011.4229 [hep-lat].
- [41] C. Schmidt [for the HotQCD Collaboration], AIP Conf. Proc. **1343** (2011) 513 [arXiv:1012.2230 [hep-lat]].
- [42] M. Cheng, N. H. Christ, S. Datta, J. van der Heide, C. Jung, F. Karsch, O. Kaczmarek and E. Laermann *et al.*, Phys. Rev. D **77** (2008) 014511 [arXiv:0710.0354 [hep-lat]].
- [43] A. Bazavov, T. Bhattacharya, M. Cheng, N. H. Christ, C. DeTar, S. Ejiri, S. Gottlieb and R. Gupta *et al.*, Phys. Rev. D **80** (2009) 014504 [arXiv:0903.4379 [hep-lat]].
- [44] S. Borsanyi, G. Endrodi, Z. Fodor, A. Jakovac, S. D. Katz, S. Krieg, C. Ratti and K. K. Szabo, JHEP **1011**, 077 (2010) [arXiv:1007.2580 [hep-lat]].
- [45] S. Borsanyi, Z. Fodor, C. Hoelbling, S. D. Katz, S. Krieg, C. Ratti and K. K. Szabo, arXiv:1005.3508 [hep-lat].
- [46] S. Borsanyi, G. Endrodi, Z. Fodor, C. Hoelbling, S. D. Katz, S. Krieg, C. Ratti and K. K. Szabo, arXiv:1109.5032 [hep-lat].
- [47] A. Bazavov, T. Bhattacharya, M. Cheng, C. DeTar, H. T. Ding, S. Gottlieb, R. Gupta and P. Hegde *et al.*, arXiv:1111.1710 [hep-lat].
- [48] E. Megias, E. Ruiz Arriola and L. L. Salcedo, Phys. Rev. D **74** (2006) 065005 [hep-ph/0412308].
- [49] T. K. Herbst, J. M. Pawłowski and B. -J. Schaefer, Phys. Lett. B **696** (2011) 58 [arXiv:1008.0081 [hep-ph]].
- [50] K. Fukushima, Phys. Rev. D **77** (2008) 114028 [Erratum-ibid. D **78** (2008) 039902] [arXiv:0803.3318 [hep-ph]].
- [51] S. Borsanyi, Z. Fodor, S. D. Katz, S. Krieg, C. Ratti and K. K. Szabo, arXiv:1109.5030 [hep-lat].
- [52] M. Cheng, P. Hegde, C. Jung, F. Karsch, O. Kaczmarek, E. Laermann, R. D. Mawhinney and C. Miao *et al.*, Phys. Rev. D **79** (2009) 074505 [arXiv:0811.1006 [hep-lat]].
- [53] S. Borsanyi, Z. Fodor, S. D. Katz, S. Krieg, C. Ratti and K. K. Szabo, arXiv:1112.4416 [hep-lat].
- [54] S. Jeon and V. Koch, Phys. Rev. Lett. **85**, 2076 (2000) [arXiv:0003168 [hep-ph]].
- [55] M. Asakawa, U. W. Heinz and B. Muller, Phys. Rev. Lett. **85**, 2072 (2000) [arXiv:0003169 [hep-ph]].
- [56] S. Chatterjee and K. A. Mohan, arXiv:1201.3352 [hep-ph].
- [57] M. A. Stephanov, K. Rajagopal and E. V. Shuryak, Phys. Rev. D **60** (1999) 114028 [hep-ph/9903292].